We are IntechOpen, the world's leading publisher of Open Access books Built by scientists, for scientists

4,800
Open access books available

122,000
International authors and editors

135M
Downloads

Our authors are among the

154
Countries delivered to

TOP 1%
most cited scientists

12.2%
Contributors from top 500 universities

CLARIVATE ANALYTICS BOOK CITATION INDEX INDEXED

WEB OF SCIENCE™

Selection of our books indexed in the Book Citation Index in Web of Science™ Core Collection (BKCI)

Interested in publishing with us?
Contact book.department@intechopen.com

Numbers displayed above are based on latest data collected.
For more information visit www.intechopen.com

19

Shape of the Coherent Population Trapping Resonances Registered in Fluorescence

Sanka Gateva and Georgi Todorov
Institute of Electronics, Bulgarian Academy of Sciences
Bulgaria

1. Introduction

There has been permanent interest in investigations of new magnetic sensors and their various applications (Edelstein, 2007). Last years there is a rapid progress in development of magneto-optical sensors because of their sensitivity and potential for miniaturization. Magnetometers, based on magneto-optical sensors have high sensitivity - comparable to, or even surpassing this of the SQUIDs (Superconducting Quantum Interference Devices) (Kominis et al., 2003; Dang et al., 2010; Savukov, 2010; Knappe, 2010). Microfabrication of components using the techniques of Micro-Electro-Mechanical Systems (MEMS) developed for atomic clocks (Knappe, 2004) gives the opportunity for building small, low consuming, low cost and non-cryogenic (as SQUIDs) sensors (Griffith et al., 2010). Coherent optical effects can be applied for magnetic field detection and offer perspectives for development of high-precision optical magnetometers (Cox et al., 2011; Kitching et al., 2011). These magnetometers are appropriate for geomagnetic, space, nuclear and biological magnetic field measurements (cardio and brain magnetic field imaging), environmental monitoring, magnetic microscopy, investigations of fundamental physics, etc. Coherent magneto-optical resonances have many applications not only in magnetometry, but in high-resolution spectroscopy, lasing without inversion, laser cooling, ultraslow group velocity propagation of light, etc. (Gao, 2009).

Magneto-optical resonances can be prepared and registered in different ways (Budker&Romalis, 2007 and references therein). Most frequently Coherent–Population-Trapping (CPT) is observed when two hyperfine levels of the ground state of alkali atoms are coupled by two laser fields to a common excited level. When the frequency difference between the laser fields equals the frequency difference between the two ground states, the atoms are prepared in a non-absorbing state, which can be registered as a fluorescence quenching and transparency enhancement in spectral interval narrower than the natural width of the observed optical transition (Arimondo, 1996).

In degenerate two-level systems coherent states can be created by means of Hanle effect configuration (Alzetta et al., 1976). In this case the coherent non-absorbing state is prepared on two Zeeman sublevels of one hyperfine level by monochromatic laser field (the so called single frequency CPT). Hanle configuration is important for performing significantly simplified experiments and to build practical devices as well.

For a lot of applications in medicine, quantum information experiments, materials characterization, read out of stored memory domains etc., magnetic field imaging is essential (Bison et al., 2009; Johnson et al., 2010; Kimble, 2008; Lukin, 2003; Mikhailov et al., 2009; Romalis, 2011; Xia et al., 2006). The most common techniques for monitoring the flow phenomena involve fluorescence detection (Xu et al., 2008) because it is sensitive, non-invasive, and allows in-line analysis of multiple step processes.

For all applications, where narrow signals and high signal-to-noise ratios are important, ensuring reliable operation requires good knowledge of the resonance shape and the internal and external factors influencing it.

In this chapter, the influence of different factors on the shape of the CPT resonances obtained by means of the Hanle effect configuration and registered in fluorescence is analysed in uncoated, room temperature vacuum cells from point of view of cell diagnostics and building high-sensitive magneto-optical sensors.

2. Shape of the single frequency CPT resonances

2.1 Experimental shapes

2.1.1 Experimental set-up

The experimental set-up geometry is shown in Fig. 1. The resonances were measured in uncoated vacuum cells containing a natural mixture of Rb isotopes at room temperature (22^{o}C). A single-frequency linearly polarized in **z** direction diode laser beam (2 mm in diameter, 22 mW in power) was propagating along the cell's axis **x**. Its frequency and emission spectrum were controlled by observing fluorescence from a second Rb vapor cell and a Fabry-Perot spectrum analyzer. A magnetic field $\boldsymbol{B}_{scan}$, created by a solenoid, was applied collinearly to the laser beam. As the shape of the CPT resonance is very sensitive to stray magnetic fields (Huss et al., 2006), the gas cell and the solenoid were placed in a 3 layer μ-metal magnetic shield. The fluorescence was detected perpendicular to the laser beam direction and to the light polarization vector (in **y** direction) by a photodiode. In all experiments it was placed close to the front window of the cell because the CPT resonances registered in fluorescence are sensitive to the position of the photodiode along the cell (Godone et al., 2002). The signals from the photodiode were amplified and stored in a PC, which also controlled the magnetic field scan. The main sources of errors were the accuracy of the laser power measurements and the poor signal-to-noise ratio at low laser powers.

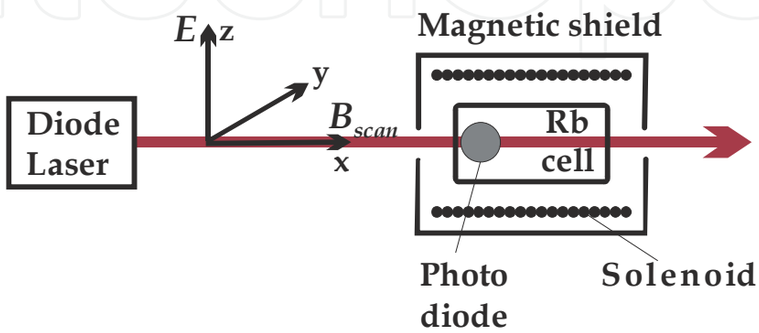

Fig. 1. Experimental setup geometry.

The resonances were examined in 4 Rb vacuum cells with internal dimensions: cell **A** (length l_A=4.5 cm, diameter d_A=2.9 cm); cell **B** (length l_B=2.0 cm, diameter d_B=2.0 cm); cell **C** (length l_C=4.4 cm, diameter d_C=1.0 cm) and cell **D** (length l_D=4.3 cm, diameter d_D=2.1 cm).

All investigations were performed on the degenerate two-level system of the (F_g=2 – F_e=1) transition of the ^{87}Rb D_1 line because the D_1 line consists of hyperfine transitions at which only dark resonances can be observed, the fluorescence of the F_g=2 – F_e=1 transition is practically not overlapping with another and it has the highest contrast (55%) (Dancheva et al., 2000).

As the spectra in the Hanle effect configuration were measured by tuning the magnetic field, all experimental spectra are plotted as function of the magnetic field. The conversion of magnetic field to frequency is straightforward on the basis of the Zeeman splitting between adjacent magnetic sublevels of the ground level ~0.7 MHz/G (Steck, 2009).

2.1.2 Experimental shapes

The measurement of the CPT resonances in four uncoated Rb vacuum cells with different dimensions (the dimensions of the cells **A**, **B**, **C** and **D** are given in Section 2.1.1) has shown that they are different not only in width but also in shape. In Fig. 2 the normalized CPT signals measured in cell **A** and cell **D** are compared in 1.25 G and 40 mG tuning ranges. In cell **A** the resonance width (FWHM) is about 50 mG, while in cell **D** it is 250 mG (Fig. 2a). In cell **D** the resonance has triangular shape (Fig. 2b scattered circles curve), while in cell **A** the resonance has a narrow Lorentzian structure of the order of few mG centred at zero magnetic field superimposed on a broad pedestal of the order of a few hundred mG (Fig. 2 dashed line curve).

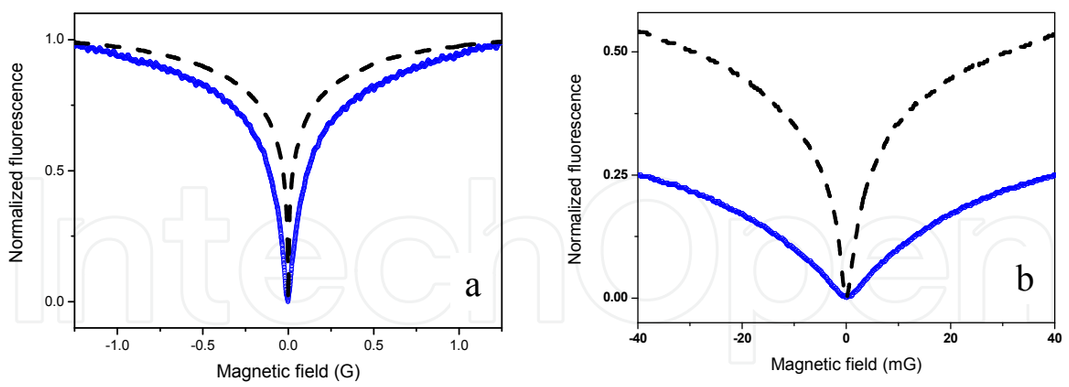

Fig. 2. Normalized CPT resonance shapes in cell **A** (dash line curve) and cell **D** (scattered circles curve) in 1.25 G (a) and 40 mG (b) tuning range. Power density 75 mW/cm².

In order to obtain information about the processes leading to the narrow structure formation, measurement of the resonance shapes in all cells in dependence on the laser beam diameter, laser power density, additional constant magnetic fields, and the laser frequency position relative to the centre of the Doppler broadened line profile were performed (Alipieva et al., 2003). The analysis of the shapes, measured at the same geometry

of excitation and registration, has shown that the origin of the narrow structure is connected with processes in the vacuum cell. The width of the resonances is different in different cells and it is about 2 orders smaller than the transit-time broadening, which is of the order of 100 kHz (Thomas & Quivers, 1980). The width of the narrow Lorentzian structure of the CPT resonance is in agreement with the assumption that the broadening is mainly affected by the relaxation processes due to atomic collisions with the walls of the cell.

In Fig. 3 the measured narrow resonance widths of the four cells are plotted as function of the mean distance between two collisions with the cell walls L. The red line is the calculated resonance width (FWHM) $\Delta_L = 1/2\pi\tau$ determined by the mean time between two collisions with the cell walls $\tau=L/v= 4V/Sv$ (Corney, 1977) where v is the mean thermal velocity, V is the volume, S is the surface area of the cell and L is the mean distance between 2 collisions with the cell walls. The time of atom-wall interaction during the collision is small enough (Bouchiat & Brossel, 1966) and is neglected. The measured values of the resonance width are in good agreement with the evaluated for three of the cells (cell **A**, **B** and **C**). Only in cell **D** there is no narrow structure and in Fig. 3 this is designated by a dashed line at the corresponding to cell **D** mean distance between collisions with the cell walls. The different dimensions of the cell can not be the reason for the existence of the narrow resonance. The estimated mean path between two collisions with the cell walls L is 2.1 cm in cell **A** and 1.6 cm in cell **D**. As the measurements are made at the same temperature, the mean velocity of the atoms is the same. Then, the evaluated difference between the widths of the eventual narrow resonances is of the order of 25-30% and is detectable.

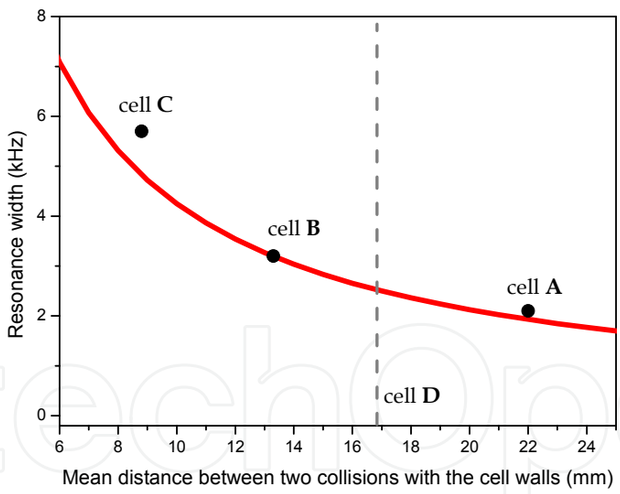

Fig. 3. FWHM of the narrow resonances (black circles) as function of the dimensions of the cell (mean distance between two collisions with the cell walls) and the calculated dependence of the width of the resonance, result of relaxation on the cell walls (red line). Laser beam diameter 2 mm, P_{las}= 75 mW/cm^2.

In Fig. 4 the power dependences of the amplitudes and widths of the narrow and the wide structures of the CPT resonances measured in cell **A** are shown. The amplitudes of both signals increase with power. The amplitude of the wide structure increases fast with power and at intensities larger than 150 mW/cm^2 saturates. The amplitude of the narrow structure is lower and does not saturate up to a power density of 1 W/cm^2.

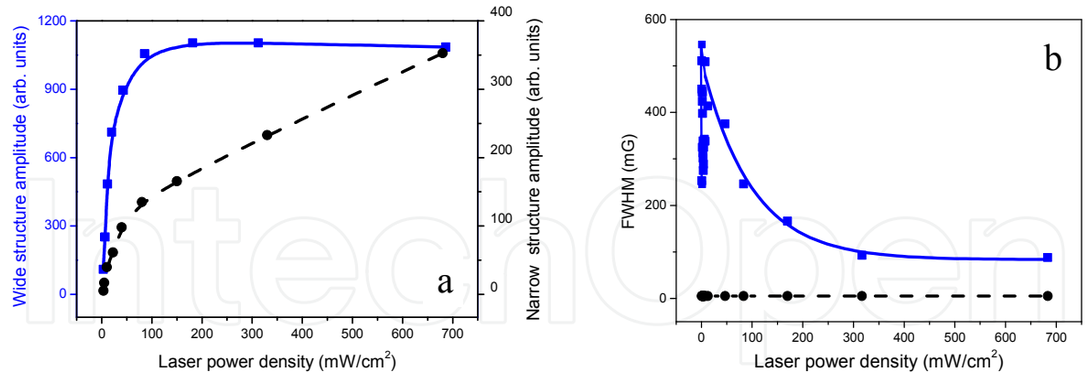

Fig. 4. Amplitudes (a) and widths (b) of the narrow (black circles) and wide (blue squares) structure of the CPT resonance in dependence on the laser power density. (The lines are only to guide the eyes.)

The width of the narrow structure does not depend on the laser power, while the wide structure width does - at low powers it increases, and at laser power densities higher than 1 mW/cm², there is no power broadening, but a resonance-line narrowing with the power - an exponential decrease to 80 mG. A possible explanation of this narrowing in our experiment is the high pumping rate. The CPT signal width is proportional to the pumping rate Ω^2/γ^* (γ^* is the total decay rate of the excited state defined not only by the spontaneous decay but by all relaxation processes) (Levi et al., 2000). When the laser power density is increased, the saturation of the absorption cannot be neglected, the decay rate of the excited state γ^* increases due to the stimulated emission and a resonance width narrowing is observed.

The comparison of the narrow structure registered in fluorescence and transmission (Gateva et al., 2005) shows that the narrow structure width is the same in fluorescence and transmission. In fluorescence, the narrow resonances can be observed in the whole range of laser powers, while in transmission, in a very small range of powers because of the absorption saturation.

The measured dual structure resonance shapes and the power dependences of the two components make reasonable the assumption that the signal in these cells is formed by different subensembles of atoms interacting with different light fields – the laser beam and a weak light field, for example, of scattered light.

This assumption is confirmed by the series of experiments with cell **A** with an expanded beam filling the whole volume of cell **A**. The dependence of the shape of the CPT resonances on the laser beam diameter is given in Fig. 5a. (The diameter of the laser beam with laser power density 0.3 mW/cm² was changed by different diaphragms in front of the cell.) The resonances broaden with decreasing the diameter, but there is a narrow range (about 3 mG in width) around the zero magnetic field, where their shapes are Lorentzian and equal in width. In the limits of the accuracy of the measurement this width is equal to the narrow component width and to the non power broadened CPT resonance of the expanded to 30 mm laser beam (Fig. 5b). In Fig. 5b the power dependence of the resonance width with

30 mm laser beam is shown. The initial intensity of the laser beam was reduced by a neutral filter from maximum to 1/128. In this case, the resonance width is determined by the relaxation processes due to atomic collisions with the walls of the cell and the power broadening.

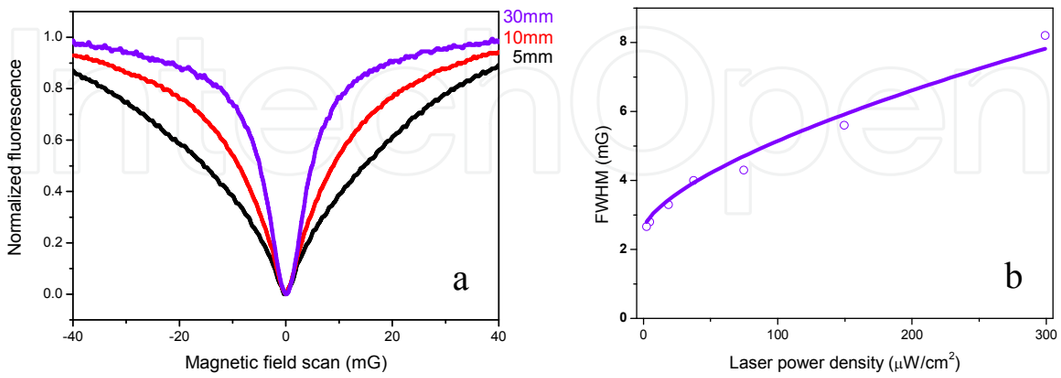

Fig. 5. CPT resonances with expanded laser beam:
(a) shape of the resonances at different diameters of the laser beam and reduced laser power density 0.3 mW/cm²;
(b) power dependence of the resonance width with 30 mm laser beam diameter.

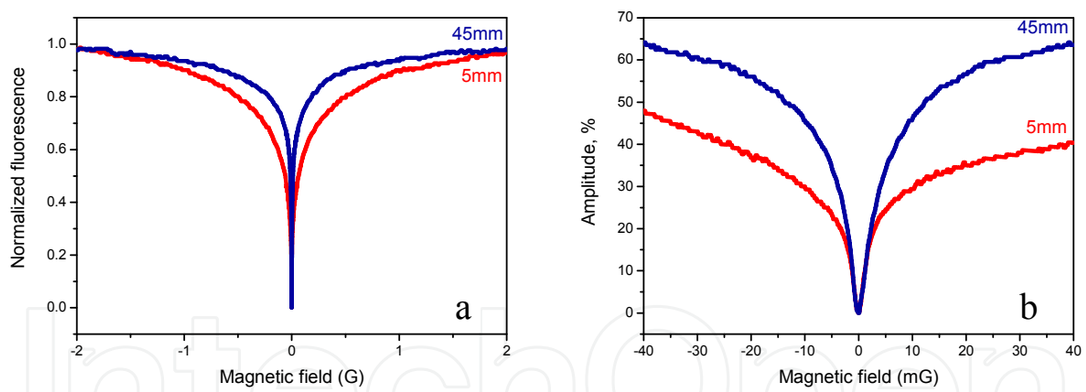

Fig. 6. CPT resonances registered at 5 mm and 45 mm along the cell in two different tuning ranges: a) 2 G and b) 40 mG. Beam diameter 2 mm.

In Fig. 6 the resonance shapes registered with laser beam diameter 2 mm at 5 mm and 45 mm distance from the input window are given. The comparison of the shapes of the resonances in a 2 G tuning range (Fig.6a) shows, that the resonance at the end of the cell is narrower. This result coincides with the theoretical and experimental results of Godone et al. (Godone et al., 2002) and is due to the lower laser power at the end of the cell and the smaller power broadening.

The comparison of the signals in a 10 mG range shows that there is a narrow range (about 3 mG in width) around the zero magnetic field, where their shapes coincide.

2.2 Theoretical description

The shape and width of the CPT resonances and their dependence on the input power has been studied experimentally and theoretically in many papers (Auzinsh, 2009a,b and references therein). Most of the experimental investigations were performed at low laser power, the shape of the resonances was Lorentzian and the dependence of the resonance width Γ on the laser power density was linear up to a few mW/cm². The slope of this dependence was smaller than the predicted by the theory (Arimondo, 1996):

$$\Gamma = \gamma_\varphi + \Omega^2/\gamma_f \tag{1}$$

where γ_φ is the ground state coherence relaxation rate; Ω, the Rabi frequency; γ_f , the population decay rate from the excited state into the ground states.

There are different decoherence processes influencing the resonance shape – transit time broadening, population exchange, atom-atom and atom-wall collisions, transverse laser intensity distribution etc. The investigations of the resonance shapes at different conditions have shown that not always the power dependence of the resonance width is linear (Figueroa et al., 2006; Javan et al., 2002; Ye&Zibrov, 2002).

An analytical expression for the FWHM of the EIT resonances Γ_{EIT} in the case of a Doppler broadened medium in the linear with respect to the probe field approximation, when the population exchange between the ground states is the main source of decoherence, was obtained by Javan et al. (Javan et al., 2002):

$$\Gamma_{EIT}^2 = \frac{\gamma_\varphi}{\gamma_f}\Omega^2(1+x)\left\{1+\left[1+\frac{4x}{(1+x)^2}\right]^{1/2}\right\} \tag{2}$$

under the condition $\left(\gamma_f / w_D\right)^2 << x << \gamma_f / \gamma_\varphi$. The parameter $x = \Omega^2 / \Omega_{in\,\mathrm{hom}}^2 = \Omega^2\gamma_f / 2\gamma_\varphi w_D^2$ represents the degree of optical pumping within the inhomogeneous linewidth w_D. The dependence of Γ_{EIT} on the laser power density is not linear at low intensities -when $x<<1$, $\Gamma_{EIT} \approx \sqrt{\frac{2\gamma_\varphi}{\gamma_f}}.\Omega$, and linear at high intensities - when x>>1, $\Gamma_{EIT} \approx \frac{\Omega^2}{w_D}$.

The investigation of the influence of the light beam transverse intensity distribution on the line shape has shown that due to the Gaussian shape of the beam, at high pumping rates the shape of the resonances is no more Lorentzian (Pfleghaar et al., 1993). The obtained by Levi et al. (Levi et al., 2000) analytical lineshape is:

$$\Pi(\delta) = \frac{1}{2}\ln\frac{\Omega^2 / \gamma_f\gamma_\varphi}{1+(\delta/\gamma_\varphi)^2} \tag{3}$$

where δ is the two-photon detuning, while by Taichenachev et al. (Taichenachev et al., 2004) it is:

$$R_G = \pi r_0^2(S_0 - \delta\ \arctan[S_0\delta/(1+S_0+\delta^2)] + \frac{1}{2}\ln\{(1+\delta^2)/[(1+S_0)^2+\delta^2]\}) \tag{4}$$

where $S_0=\frac{\Omega^2}{\gamma_f \cdot \gamma_\varphi}$.

At high power densities (S_0>>1) it is

$$R_G \propto \{1-(\delta/S_0)\ \arctan(S_0/\delta)\} \tag{5}$$

These equations describe well the standard (bichromatical) CPT resonance registered in absorption.

To understand the reason for the observed peculiarities in the shapes and widths of the Hanle - CPT resonances in different cells we have performed a numerical modelling of the influence of the experimental conditions. The theoretical description is based on the standard semiclassical approach: the atomic system is described by the statistical operator $\hat{\rho}$ in density matrix representation (Landau & Lifshitz, 1965) and laser and magnetic fields are considered classically.

The Hamiltonian of the system $\hat{H}$ is sum of the operator of the free atom $\hat{H}_0$, the operator of magneto-dipole interaction $\hat{H}'$ and the operator of interaction with the laser radiation $\hat{V}$. Terms describing the atomic relaxation and excitation transfer are added to the Liuville/Neuman equation:

$$\dot{\hat{\rho}} = -\frac{i}{h}\left[\hat{H},\hat{\rho}\right] + \left(\dot{\hat{\rho}}\right)_{relax} + \left(\dot{\hat{\rho}}\right)_{tr} + \hat{N} \tag{6}$$

where $\hat{H} = \hat{H}_0 + \hat{H}' + \hat{V}$.

At weak magnetic fields the magneto-dipole interaction is smaller than the hyperfine splitting and the hyperfine splitting can be included in the main Hamiltonian $\hat{H}_0$. In this case the magneto-dipole operator can be written as: $\hat{H}' = \mu_B g_{F_S}\left[\vec{F}_s,\vec{H}\right]$, where μ_B is the Bohr magneton, g_{F_s} is the Lande factor, F_s is the total moment of the atom in the s state, ($s = f,\varphi$; f - upper, φ - lower state), and $\vec{H}$ is the vector of the magnetic field. The complete magnetic field includes the scanning magnetic field and a residual magnetic field H_{str} .

The operator of interaction with the laser radiation $\hat{V}$ is described with the scalar product of the vector operator of the dipole moment $\vec{d}$ and the electric vector $\vec{E}$ of the resonant to the atomic transition $\varphi \to f$ light:

$$\hat{V} = -\left(\vec{d}.\vec{E}\right), \qquad \vec{E} = E\vec{e}_Q \exp\{-i(\omega_{las}t - kz)\} + c.c. \tag{7}$$

where: $\vec{e}_Q$ $(Q = 0,\pm 1)$ are the circular components of the laser field, ω_{las} is the frequency of the laser light and $\vec{k}$ is the wave vector.

Applying the irreducible tensor operator (ITO) formalism, the density matrix $\rho_{nn'}$ in (n,n′) representation can be decomposed into polarization moment (PM) representation with tensor components ρ_q^k (Dyakonov & Perel, 1966)

$$\rho_q^k = (2F_{\rho'}+1)^{1/2}\sum_{n,n'}(-1)^{F_\rho - n}\begin{pmatrix} F_\rho & k & F_{\rho'} \\ -n & q & n' \end{pmatrix}\rho_{nn'} \tag{8}$$

Here $\rho = f,\varphi,\xi$ denote the components (f_q^k) and (φ_q^k) of the upper *(f, F_f)* and lower (φ, F_φ) levels respectively and the optical components (ξ_q^k).

The parentheses denote the 3j-symbol. Since q =n - n′, the ρ_q^k components with q = 0 are linear combination of the sublevels population. For example, for k=0, $\rho_0^0 = \sum_n \rho_{nn}$ is the total population and for *k*=2, q=0, $\rho_0^2 = \sum_{n=-F_\rho}^{F_\rho} f_{nn}\frac{3n^2 - F_\rho(F_\rho+1)}{[(2F_\rho+3)(F_\rho+1)(2F_\rho-1)\}^{1/2}}$ is the longitudinal alignment, etc.

The relaxation of the atomic system is described phenomenologically by sum of two terms and in the common case includes radiation and collisional processes. Besides the clear physical meaning of the tensor components in this (*k,q*) representation, the relaxation matrix is diagonal in the main cases and all relaxation parameters for different ρ, $\gamma_\rho(k,q) = \gamma_\rho(k)$ $(\rho = f,\varphi,\xi)$ for the k-th tensor component of the upper (*f*) and lower (φ) levels and the decay of the optical coherence (ξ) depend on the rank *k* of the components only. The decay of the lower level $\gamma_\varphi(0)$ includes the time-of-flight influence. The second term $(\dot{\hat{\rho}})_{tr}$ describes the excitation transfer by spontaneous emission $\Gamma_{F_f F_\varphi}(\kappa)$ from the upper level to the lower one and includes the transfer of Zeeman coherence.

According to Ducloy & Dumont (Ducloy & Dumont, 1970) and taking into account Dyakonov & Perels's normalization of the irreducible tensor operators (Dyakonov & Perel, 1966)

$$\begin{aligned}\Gamma_{F_f F_\varphi}(k) = (-1)^{F_f+F_\varphi+k+1}[\gamma_f(0)(2F_f+1)(2F_\varphi+1)(2J_f+1)]\cdot \\ \cdot\begin{Bmatrix} F_f & F_\varphi & 1 \\ J_\varphi & J_f & I \end{Bmatrix}^2\sqrt{(2F_f+1)(2F_\varphi+1)}\begin{Bmatrix} F_f & F_f & k \\ F_\varphi & F_\varphi & 1 \end{Bmatrix}\end{aligned} \tag{9}$$

Here $\gamma_f(0)$ is the total probability of decay of the upper state to the lower states.

It is worth to note that the relaxation constant $\Gamma_{F_f F_\varphi}(k)$ describes the "losses" in the channel $F_f \to F_\varphi$. If the branching ratio $\Gamma_{F_f F_\varphi}(0)/\gamma_f(0)$ is close to 1, the atomic system is closed. In the particular case of ^{87}Rb D_1 line transition $F_f = 1 \to F_\varphi = 2$, the ratio $\Gamma_{F_f F_\varphi}(0)/\gamma_f(0)$ =5/6.

For the matrix element of the dipole transitions between hf states in ITO representation one can write (Alexandrov et al., 1991):

$$d_{F_f F_\varphi} = \|d_{f\varphi}\|(-1)^{2F_\varphi+J_f+I+1}\left[(2F_f+1)(2F_\varphi+1)\right]^{1/2}\begin{Bmatrix} I & J_f & F_f \\ 1 & F_\varphi & J_\varphi \end{Bmatrix}(-1)^{F_\varphi+m}\begin{Bmatrix} F_\varphi & 1 & F_f \\ -m & Q & \mu \end{Bmatrix}e_Q \tag{10}$$

The brackets denote 6j-Wigner symbols, $\|d_{f\varphi}\|$ is the reduced matrix element of the dipole $F_f \to F_\varphi$ transition.

The initial conditions are defined by the operator $\hat{N} = N_s(2F_s + 1)W(\mathrm{v})$, which describes the population of the resonant to the laser light levels. It is supposed that the atomic ensemble is in equilibrium and the velocity distribution of the atoms is described by a Maxwell function $W(v)$.

$$W(v) = (u\sqrt{\pi})^{-1} e^{(-v^2/u^2)} \tag{11}$$

Taking into account the stated above, the system of equations describing the ground state (φ), the exited state (f) and the optical coherency (ξ) for arbitrary angular moments is:

$$\begin{aligned} &\dot{f}_q^k + \gamma_f(k) f_q^k = i\mu_B g_f h^{-1} \left\{ qH_0 f_q^k + \left[\frac{1}{2}(k+q)(k-q+1) \right]^{1/2} H_1 f_{q-1}^k - \right. \\ &\left. - \left[\frac{1}{2}(k-q)(k+q+1) \right]^{1/2} H_{-1} f_{q+1}^k \right\} + L_q^k + (2F_f + 1) N_f W(\nu) \delta_{k0} \delta_{q0} \end{aligned} \tag{12a}$$

$$\begin{aligned} &\dot{\varphi}_q^k + \gamma_\varphi(k) \varphi_q^k = i\mu_B g_\varphi h^{-1} \left\{ qH_0 \varphi_q^k + \left[\frac{1}{2}(k+q)(k-q+1) \right]^{1/2} H_1 \varphi_{q-1}^k - \right. \\ &\left. - \left[\frac{1}{2}(k-q)(k+q+1) \right]^{1/2} H_{-1} \varphi_{q+1}^k \right\} + M_q^k + (2F_\varphi + 1) N_\varphi W(\nu) \delta_{k0} \delta_{q0} + \Gamma_{F_f F_\varphi}(k) f_q^k \end{aligned} \tag{12b}$$

$$\begin{aligned} &\dot{\xi}_q^k + \left(\gamma_\xi(k) + i\omega_0 \right) \xi_q^k = ih^{-1} \sum_{k'Q} (-1)^Q H_{-Q} (-1)^{F_f + F_\varphi + q} (2k'+1) \begin{pmatrix} k' & 1 & k \\ -q' & Q & q \end{pmatrix} \\ &\left[\mu_B g_\varphi \left(\varphi \| j \| \varphi \right) \begin{Bmatrix} F_f & F_\varphi & k' \\ 1 & k & F_\varphi \end{Bmatrix} + (-1)^{k+k'} \mu_B g_f \left(f \| j \| f \right) \begin{Bmatrix} F_\varphi & F_f & k' \\ 1 & k & F_f \end{Bmatrix} \right] \xi_{q'}^{k'} + G_q^k \end{aligned} \tag{12c}$$

Where:

$$L_q^\kappa = ih^{-1} (2\mathrm{F}_\varphi + 1)^{-1/2} \sum_{\kappa' q' Q} E_{-Q} \mathrm{C}_{qq'Q}^{\kappa\kappa'} \left[\mathrm{d} \xi_{q'}^{\kappa'} + \mathrm{d}^* (\xi_{q'}^{\kappa'})^* (-1)^{\kappa+\kappa'+q'} \right]$$

with $\mathrm{C}_{qq'Q}^{\kappa\kappa'} = (-1)^{2\mathrm{F}_\varphi + q'} (2\mathrm{F}_f + 1)^{1/2} (2\kappa' + 1) \begin{Bmatrix} \kappa' & 1 & \kappa \\ F_f & F_f & F_\varphi \end{Bmatrix} \begin{pmatrix} k' & 1 & \kappa \\ -q' & Q & q \end{pmatrix}$;

$$M_q^\kappa = (-1)^\kappa ih^{-1} (2\mathrm{F}_\varphi + 1)^{-1/2} \sum_{\kappa' q' Q} E_{-Q} (-1)^{\kappa'} \mathrm{B}_{qq'Q}^{\kappa\kappa'} \left[\mathrm{d} \xi_{q'}^{\kappa'} + \mathrm{d}^* (\xi_{q'}^{\kappa'})^* (-1)^{\kappa+\kappa'+q'} \right]$$

with $\mathrm{B}_{qq'Q}^{\kappa\kappa'} = (-1)^{2\mathrm{F}_\mathrm{f} + q'} (2\mathrm{F}_\varphi + 1)^{1/2} (2\kappa' + 1) \begin{Bmatrix} \kappa' & 1 & \kappa \\ F_\varphi & F_\varphi & F_f \end{Bmatrix} \begin{pmatrix} \kappa' & 1 & \kappa \\ -q' & Q & q \end{pmatrix}$;

$$G_q^\kappa = ih^{-1} (2\mathrm{F}_f + 1)^{-1/2} \mathrm{d}^* \sum_{\kappa' q' Q} E_{-Q} \left[\mathrm{S}_{qq'Q}^{\kappa\kappa'} f_{q'}^{\kappa'} + (-1)^{\kappa+\kappa'} \mathrm{R}_{qq'Q}^{\kappa\kappa'} \varphi_{q'}^{\kappa'} \right]$$

with $R^{\kappa\kappa'}_{qq'Q} = (-1)^{2F_\varphi+q'}(2F_f+1)^{1/2}(2\kappa'+1)\begin{Bmatrix}\kappa' & 1 & \kappa\\ F_f & F_\varphi & F_\varphi\end{Bmatrix}\begin{pmatrix}\kappa' & 1 & \kappa\\ -q' & Q & q\end{pmatrix}$

and $S^{\kappa\kappa'}_{qq'Q} = (-1)^{2F_f+q'}(2F_\varphi+1)^{1/2}(2\kappa'+1)\begin{Bmatrix}\kappa' & 1 & \kappa\\ F_\varphi & F_f & F_f\end{Bmatrix}\begin{pmatrix}\kappa' & 1 & \kappa\\ -q' & Q & q\end{pmatrix}$

Here ω_0 is the resonance frequency for the given transition and $d \equiv \|d_{f\varphi}\|$, $(\rho\|j\|\rho) = [(2F_\rho+1)(F_\rho+1)F_\rho]^{1/2}$.

This basic system of equations (Eqs. 12) is practically analogous to the well known equations (Decomps et al., 1976; Dyakonov&Perel, 1966).

The system of Eqs. 12 is specified for the atomic transition F_f=1→F_φ=2 and the experimental geometry. The quantization axis is chosen parallel to the electric vector $E(\equiv E_z=E_0)$ of the laser field (see the experimental setup in Fig. 1). The scanned magnetic field $\boldsymbol{H}_{scan}(\equiv H_x)$ is perpendicular to this axis. The influence of the laboratory magnetic field is taken into account including two orthogonal components H_z and H_y into the equations.

Using a rotating wave approximation (RWA) and assuming a single-frequency laser field (Eq. 7), the system of equations is reduced to an algebraic one. The obtained system of equations is solved numerically at different parameters: Rabi frequency ($\Omega = d \cdot E/\hbar$), relaxation constant of the levels f and φ $((\gamma_f(k), \gamma_\varphi(k))$, spontaneous emission transfer coefficients $\Gamma_{f\varphi}(k)$ and stray field components (H_y, H_z). All these parameters and the magnetic fields are expressed in units $\gamma_f(0)$. The initial (unbroadened by the laser field) low level population relaxation rate constant $\gamma_\varphi(0)$ is determined by the time of flight of the atoms. To describe better the experimental conditions the program is additionally modified to take into account the Gaussian intensity distribution of the irradiating beam and the Maxwell velocity distribution of the atoms. The solution for a given variable (ρ^k_q) is taken after summarizing the partial solutions for the sub-ensemble of atoms with velocities in a given interval. The integration step is varied and the integration region is chosen to be > 40 $\gamma_f(0)$. The obtained solutions for a given power are summarized on the laser beam intensity distribution.

The intensity of the registered in our experiments fluorescence $I_{F_eF_g}(\vec{n}(\theta,\varphi))$ from the upper to the lower level in direction $\vec{n}(\theta,\varphi)$ is described with:

$$I_{F_fF_\varphi}(\vec{n}) = C_0(-1)^{F_e+F_g}(2F_f+1)^{-1/2}\left|d^2_{f\varphi}\right|\sum(2\kappa+1)\begin{Bmatrix}1 & 1 & \kappa\\ F_f & F_f & F_\varphi\end{Bmatrix}\sum_q(-1)^q f^\kappa_q \Phi^\kappa_{-q}(\vec{n}(\theta,\varphi)) \qquad (13)$$

where f^k_q are the tensor components describing the upper level, $\Phi^\kappa_q(\vec{n}(\theta,\varphi))$ is the observation tensor (Alexandrov et al., 1991), θ is the angle between the laser light polarization and the direction of registration (the inclination angle) and φ is the azimuth angle (Alexandrov et al., 1991; Dyakonov&Perel, 1966).

In a dipole approximation the fluorescence is defined only by the tensor components f^k_q with rank $k \le 2$. The unpolarized fluorescence intensity $I^{unpol}_{f\varphi}$ for θ=0 can be written as:

$$I_{f\varphi}^{unpol} = C_0[\frac{f_0^0}{\sqrt{2F_f+1}} + (-1)^{F_f+F_\varphi+1}\sqrt{30}\begin{Bmatrix} 1 & 1 & 2 \\ F_f & F_f & F_\varphi \end{Bmatrix} f_0^2] \quad (14)$$

Only the two tensor components for the upper level f_0^0 and f_0^2 describe the signal observed in this case. In linear approximation, both components do not depend on the magnetic field. The magnetic field dependence is a result of the transfer of coherence created on the low level and it is a typical nonlinear effect.

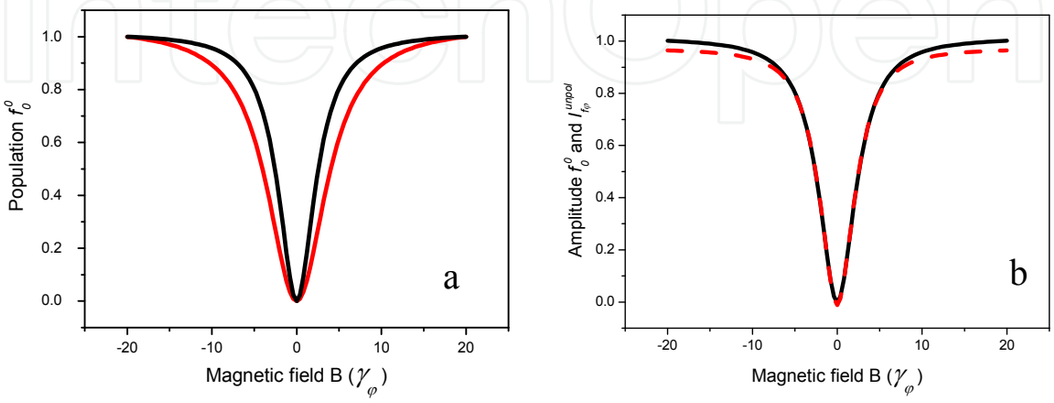

Fig. 7. Comparison of the theoretical upper level population f_0^0 : (a) calculated with (black line) and without (red line) integration over the Doppler velocity distribution and (b) with the unpolarized intensity $I_{f\varphi}^{unpol}$ (dashed red line).

It is well known that the Maxwell velocity distribution leads to narrowing of the CPT resonance (Firstenberg et al., 2007) and that the resonance shape remains quasi Lorentzian. The change in the upper level population shape and width after velocity integration over the Doppler distribution is illustrated in Fig. 7a (Petrov et al., 2007).

The main part of the unpolarized fluorescence intensity is determined by the upper level population f_0^0. The influence of the longitudinal alignment f_0^2 on the resonance shape is mainly on the wings of the resonance (Fig. 7b). It should be noted that the comparison of the numerical calculated shape of the population and intensity with a Lorentzian shape shows that there is a small specific structure in the vicinity of the zero magnetic field. This small structure is result of the High Rank Polarization Moments (HRPM) influence on the observables tensor components (see bellow).

The influence of the Gaussian distribution of the laser beam intensity on the shape of the CPT resonances is more essential. This has been discussed in a large number of papers (Knappe et al., 2001; Levi et al., 2000; Pfleghaar et al., 1993; Taichenaichev et al., 2004) and we will not illustrate it here.

The photon reabsorption is not included in this model, because in our experiments the medium is optically thin on the length scale of the laser light-atom interaction zone (Matsko et al., 2001).

The numerically calculated resonance shape which takes into account the Gaussian distribution of the laser beam intensity, the experimental geometry of the excitation and

the velocity distribution of the atoms coincides with the shape of the fluorescence resonance in cell **D** (Fig. 8a) and the pedestal of the resonance in cell **A** (Fig. 8b). This shape is in very good coincidence with the shape calculated with Eq. 5 (Taichenaichev et al., 2004). The difference between the experimental and theoretical shapes in cell **A** (Fig. 8b) is practically a Lorentzian which width is of the order of $\Delta_L=1/(2\pi\tau)$, defined by the mean time τ between two atom collisions with the cell's walls. This is the narrow structure from Fig. 2.

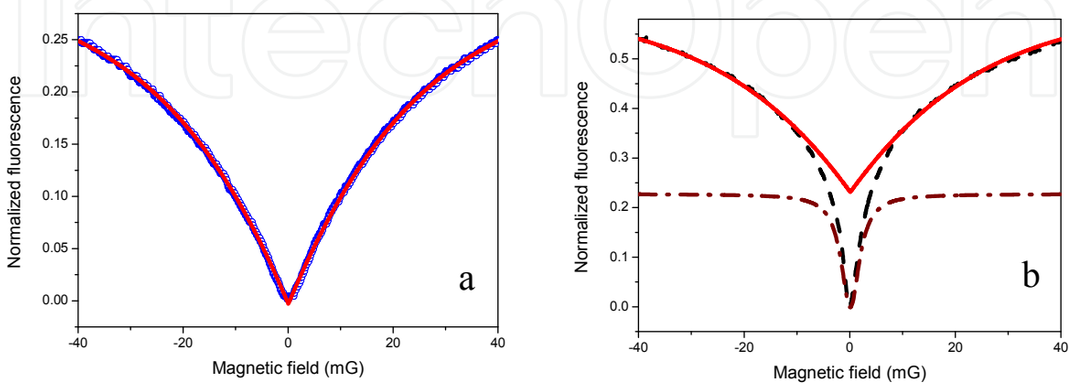

Fig. 8. Comparison of the experimental shapes with theoretical shapes:
a) experimental in cell **D** (scattered circles curve) and theoretical (solid curve);
b) experimental in cell **A** (dash line curve), theoretical (solid curve) and the difference between them (dash-dot line curve).

The comparison of the theoretical and experimental shapes in Fig. 8a shows that there is a small difference around zero magnetic field. Similar difference between the theoretical and experimental shapes was reported earlier (for example Pfleghaar et al., 1993; Taichenachev et al., 2004) and in all these cases the influence of the HRPM was not taken into account.

When the laser power density (the resonance excitation) is increased, together with the transfer of the quadrupole coherence from the ground to excited state, the influence of the multiphoton interactions will increase and high order (high rank) coherences will be created.

Our theoretical evaluations of the influence of the HRPM on the shape of the CPT resonances (Gateva et al., 2007, 2008a) proved that HRPM conversion (Okunevich, 2001) cause the CPT resonance shape peculiarities at the center of the resonance.

For a plane wave the difference from the Lorentzian shape is small and it is only around the center (at 0 magnetic field) of the resonance, with the shape and amplitude of this difference corresponding to multiphoton resonances. Although the moments of rank 4 (hexadecapole moments) (Decomps et al., 1976) do not influence directly the spontaneous emission, they are converted into the f_q^2 components of the upper level of rank 2 thus influencing the spontaneous emission.

In Fig. 9 the scheme of the connection of different rang polarization moments and the "conversion path" in population and longitudinal alignment for our scheme of excitation is illustrated (Polischuk et. al., 2011).

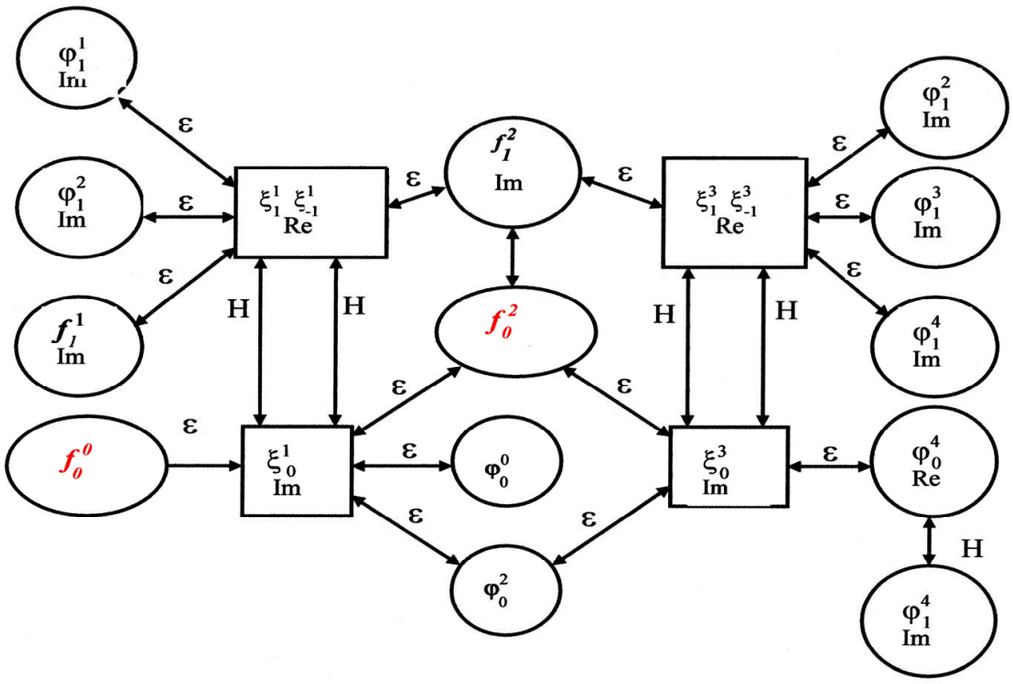

Fig. 9. Partial diagram of the mutual conversion of the tensor components forming the population (f_0^0) and the longitudinal alignment (f_0^2) (ε describes the interaction with the laser field, H – with the scanned magnetic field).

In Fig. 10 the calculated shape of the CPT resonances at different Rabi frequencies is given. At relatively low powers (Fig. 10, curve 1) the shape is close to Lorentzian; as the power is increased, the resonance flattens at the centre and an inverse narrow structure appears (Fig. 10, curves 2-4).

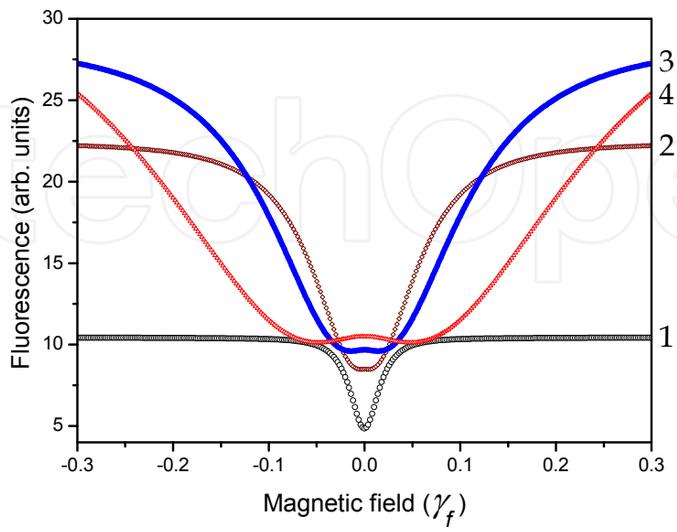

Fig. 10. Calculated shape of the CPT resonances at different Rabi frequencies $\Omega=\gamma_f$(1); $\Omega=3\gamma_f$ (2); $\Omega=5\gamma_f$(3); $\Omega=10\gamma_f$(4).

At low power density of 1.7 mW/cm² (for a laser line width 50 MHz, corresponding to reduced Rabi frequency Ω=1 MHz), the measured CPT resonance shape can not be visually distinguished from a Lorentzian, but in the difference between the experimental shape and its Lorentzian fit there is a specific structure at the center of the shape (Fig. 11a). This structure is similar to the difference between the calculated resonance and its Lorentzian fit at Ω=1 MHz (Fig. 11b).

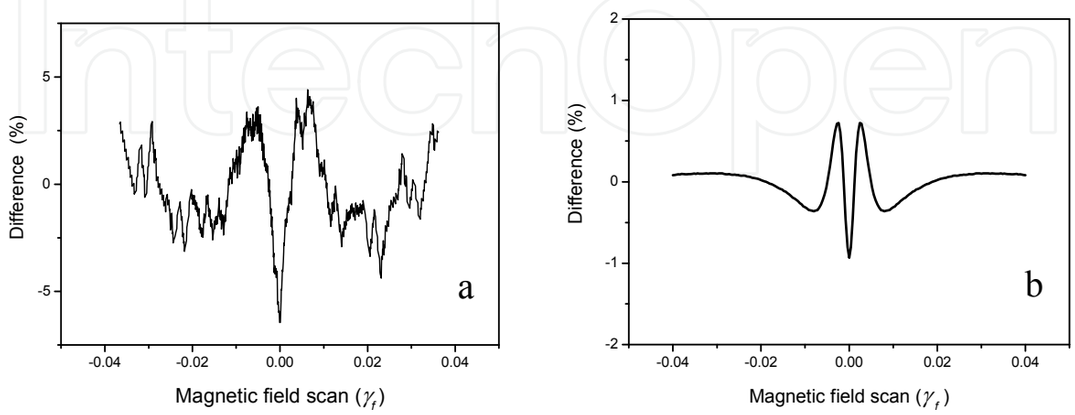

Fig. 11. Difference between:
(a) the experimental resonance shape and its Lorentzian fit
(b) the calculated resonance shape and its Lorentzian profile fit (b) at Ω=1 MHz. (The magnetic field scan is presented in γ_f units (γ_f =6 MHz is the radiation width of the upper level).

In the case of a strong laser field, at power density 1 W/cm² (corresponding to a reduced Rabi frequency Ω =25 MHz), when the measured resonance has a complex shape, the comparison of the experimental and theoretical shapes is more complicated because the amplitude of the narrow resonance increases with power (Section 2.1.2).

To observe the influence of the HRPM, the narrow structure must be eliminated. As the narrow structure is very sensitive to magnetic fields perpendicular to the polarization vector $\boldsymbol{E}(\equiv E_z)$ and $\boldsymbol{B}_{scan}(\equiv B_x)$ (Alipieva et al., 2003), magnetic fields B_y of the order of 10 mG destroy it, while the theoretical evaluations and experimental results show, that at this magnetic fields the changes in the broader structure due to the HRPM influence are practically not affected. The comparison of the shape of the resonances observed at B_y=0 (Fig. 12 curve 1) and the shape of the resonance at 32 mG (Fig. 12 curve 2) shows that at this power density the amplitude of the CPT resonance in a magnetic field is reduced twice and an additional inverted structure (about 5% in amplitude) is observed. At higher magnetic fields this inverted structure disappears (Fig. 12, curve 3).

The developed numerical model which takes into account the geometry of the excitation, the velocity distribution of the atoms and the Gaussian distribution of the laser beam intensity describes only the broad pedestal, not the narrow component from Section 2.1.2. The observed in fluorescence narrow structure of the resonance is with Lorentzian shape, it is not radiation broadened and its amplitude increases with the laser power. Its width (FWHM) Δ_L does not change with the laser beam diameter and corresponds to a relaxation time, equal to that due to atomic collisions with the cell walls.

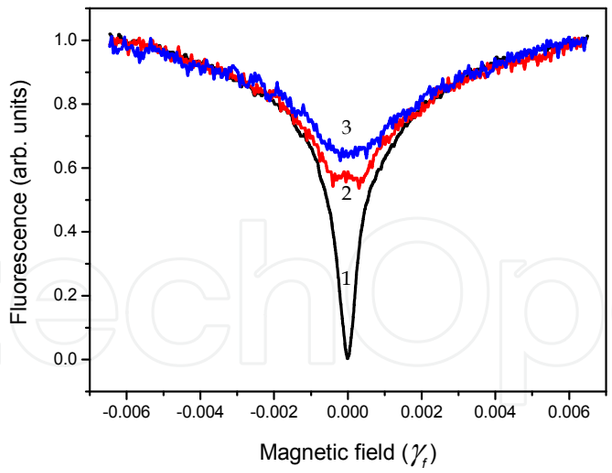

Fig. 12. CPT signals measured at different transverse to the polarization vector and propagation direction magnetic field B_y: 0 mG (curve 1); 32 mG (curve 2); 72 mG (curve 3).

Narrow structures in the CPT resonances are reported as result of diffusion-induced Ramsey narrowing (Xiao et al., 2006, 2008). In this case a sharp central peak on a broad pedestal was observed in the Electromagnetically Induced Transparency (EIT) resonance shapes. The broad pedestal is associated with the single pass interaction time and is power broadened. The sharp central peak is the central Ramsey fringe, which adds coherently for all Ramsey sequences. Its width changes with the laser beam diameter. At low laser power, small beam diameter and low buffer gas pressure the sharp central peak is not Lorentzian in shape and is insensitive to power broadening. At high laser intensity the central peak loses its contrast and is Lorentzian in shape and power broadened.

The described characteristics of the narrow structure in Fig. 2 and 8 show that it is not result of diffusion-induced Ramsey narrowing. The resonance shapes, measured at different geometries of excitation and registration (Gateva et al., 2008b, 2011), show that the narrow structure at the centre of the resonance can be considered as a result of a weak field – atom interaction, probably scattered light in the whole cell volume.

One of the possible scattering processes influencing the CPT resonance shape is Rayleigh scattering because in this case the scattered light maintains coherence with the incident beam and in this way a diffusion of the coherent light is created. For example, Rayleigh scattering has been used for studying the properties of cold atoms (Datsyuk et al., 2006) and optical lattices (Carminati et al., 2003 and references therein).

2.3 CPT resonances and Rayleigh scattering

For linear polarization of the incident light, the power of the Rayleigh-scattering light P_R registered at 90° to the laser beam direction is (Boyd, 1992; Measures, 1984)

$$P_R(\lambda,\theta) = P_0\, \alpha\, N\, \sigma(\lambda) \sin^2\theta \tag{15}$$

where P_0 is the incident light power, α is the registration efficiency coefficient, N is the scattering particles density, $\sigma(\lambda,\theta) = \sigma(\lambda) \sin^2\theta$ is the differential cross-section of Rayleigh

scattering of polarized light with wavelength λ in the plane perpendicular to the beam direction and θ is the angle between the laser light polarization and the direction of registration. According to Equation (9) the Rayleigh scattering light has a maximum at θ =90o and is zero at θ =0o.

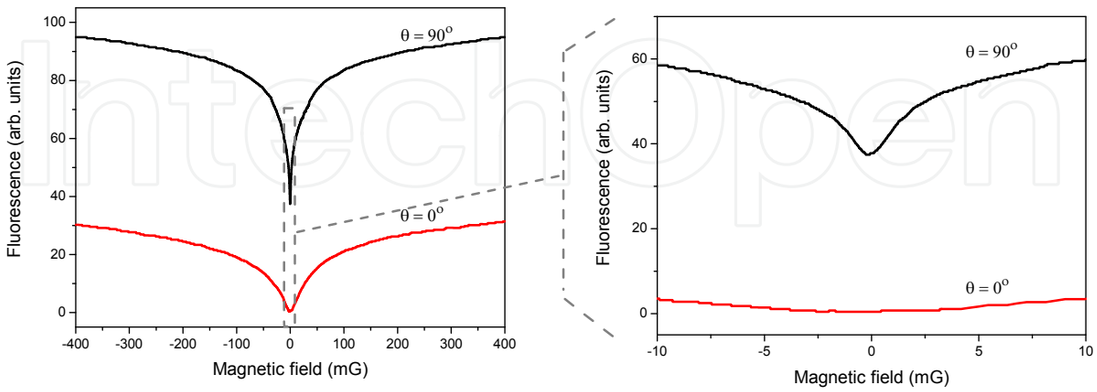

Fig. 13. Shape of the measured CPT resonances given in two different scales at angles θ =0o and 90o.

In Fig. 13 are given the shapes of the CPT resonances measured at angles θ =0o and 90o when the laser is tuned on the F_g =2 – F_e =1 transition of the ^{87}Rb D_1 line. The results are presented in two different scales. The comparison of the resonances on the broader scale shows that at the wings they are with the same shape and that this shape is in good coincidence with the calculated with the model from Section 2.2.

The comparison of the shapes in Fig. 13 on the narrower scale shows, that at θ =90o there is a narrow structure. This narrow structure is Lorentzian in shape with width of the order of the defined by the mean time between 2 collisions with the cell walls Δ_L. The amplitude of this narrow structure (Fig. 14a) has the typical $\sin^2\theta$ dependence on θ and it is maximum at θ =90o and minimum at θ =0o.

In Rb vacuum cell at room temperature the Rb pressure is of the order of 4.10^{-5} Pa and at this pressure the Rayleigh scattered light from Rb atoms can not be registered in our experiment (Boyd, 1992; Measures, 1984) – this is the case of cell **D**. However, if the vacuum cell is not pumped very well, there will be some residual air, water and oil vapor, as well as rare but relatively strongly scattering submicron particles, which will scatter the light – this is the case of cells **A**, **B** and **C**. These cells are very old (more than 20 years), manufactured with an oil diffusion pump connected by a liquid nitrogen cold trap to the cell. Cell **D** is a new one, which was sealed off some months before the experiments. It was manufactured using an oil-free vacuum installation – a turbomolecular pump and ion pump. Checking the vacuum with a Tesla coil (high voltage transformer) shows that there is no light emission (glowing) in cell **D,** while the cell glass is glowing in cell **A**, cell **B** and cell **C**.

A demonstration of the existence of Rayleigh scattered light is the measured angular dependence of the scattered light power when the laser is tuned out of line. It has the typical $\sin^2\theta$ dependence from Equation 9 with maximum at θ =90o and minimum at θ =0o (Fig. 14b).

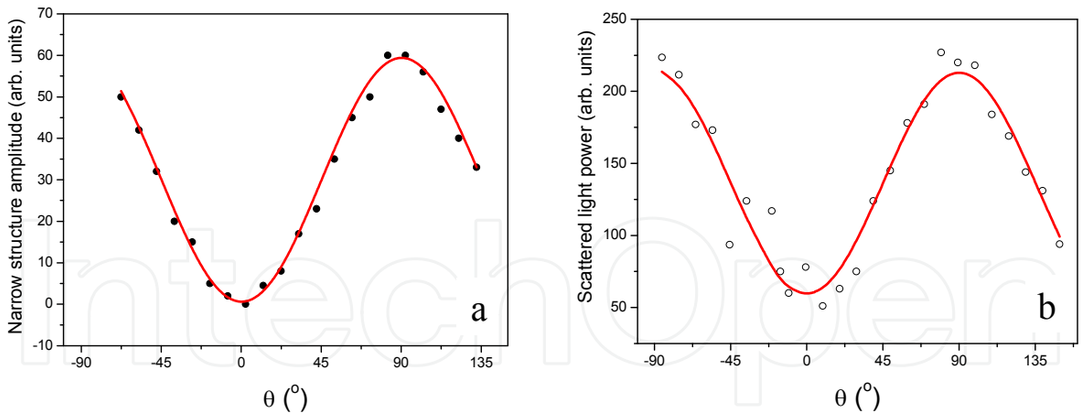

Fig. 14. Angular dependence on θ, the angle between the direction of observation and laser light polarization at 90° to the laser beam of:
(a) the narrow Lorentzian structure amplitude;
(b) the measured scattered light power when the laser is out of line.

Qualitatively, the observed narrow resonance can be described by including into the numerical model from Section 3.2 a weak, resonant, polarized light field in the cell volume. Such an approach corresponds to the supposition that the signal in the cell is formed by two subensembles of atoms interacting with different light fields. The general solution for the fluorescence intensity is sum of the numerical integrations of the density matrix equations for each of the subensembles.

For the subensemble interacting with the laser beam the evaluations following the model described in Section 2.2 have shown that this part of the signal practically does not depend on the observation direction. Although the components of the observation tensor $\Phi_q^2(\vec{n})$ depend on the direction of observation, the performed evaluations for the investigated transition have shown that the main contribution to the intensity of the unpolarized fluorescence has the population f_0^0 and $I_{F_f F_\varphi}$ practically does not depend on the observation direction.

For the subensemble interacting with the weak Rayleigh scattered light, the angular distribution of the Rayleigh scattered light has to be included in the excitation tensor. This angular dependence in the excitation reflects on all tensor components f_q^k and in this way on the fluorescence signal $I_{F_f F_\varphi}(\vec{n})$.

As the scattered light is very low in power, the resonances are with Lorentzian shape and not power broadened. When the Rabi frequency of the light field Ω is small enough, so that $\Omega^2 / \gamma_f < \gamma_\varphi$ (Eq. 1), there is no power broadening. So long as the mean free path of the atom is longer than the cell dimensions, γ_φ is defined by the mean time between two successive collisions with the cell walls. Since the weak field is due to Rayleigh scattering, the amplitude of the Lorentzian will depend on the density of the scattering particles and can be used as indicator of the level of the vacuum cleanness of the cell.

Another confirmation that the shape of the resonances is sum of the resonance shapes of different subensembles of atoms is done in experiment where the shape of the resonances

is measured at two different geometries of observation (Gateva et al., 2008b, 2011). In the first case, the photodiode is on the cell wall and the observation field of view is considerably larger than the laser beam diameter (Fig. 15, solid curve), but the angle of view is sufficiently small to ensure satisfactory angular resolution of observation. In the second case a lens is used in front of the photodiode in order to restrict the observation field of view just to the laser beam volume (Fig. 15, scattered circles curve). Because of the limited dimensions of the μ-metal shield, these measurements were performed in a smaller cell, cell **B**. The comparison of the shape of the resonances in these two cases shows that the broad pedestal doesn't change, while the shape and the width of the narrow structure change (Fig. 15). In the first case (Fig. 15, solid curve), when the fluorescence mostly of atoms out of the laser beam is registered, the narrow structure is Lorentzian in shape and its width Δ_L is defined by the relaxation on the cell walls. In the second case (Fig. 15, scattered circles curve), when fluorescence mostly from the laser beam volume is registered, the measured narrow structure is narrower than Δ_L. For explanation of such narrowing the influence of the diffusion-induced Ramsey narrowing (Xiao et all., 2006), which is result of the impurities in the cell and/or on the cell walls, has to be taken into account. Diffusion induced Ramsey narrowing resonances have been measured in Na vacuum cell, too (Gozzini et al., 2011).

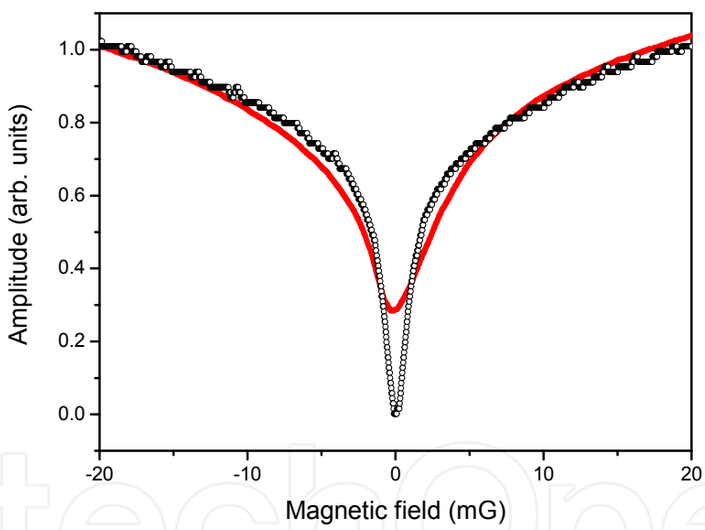

Fig. 15. Narrow structure of the CPT resonance at different geometries of registration: when the photodiode is on the cell wall (solid curve) and when the laser beam is projected by a lens on the photodiode (scattered circles curve).

This experiment can explain the difference in the narrow resonance shapes in the works of Alipieva et al. and Xiao et al. (Alipieva et al., 2003; Xiao et al., 2006). When the resonance is registered in transmission (EIT) only atoms from the laser beam volume contribute to the signal. In this case the diffusion-induced Ramsey narrowing is responsible for the narrow structure. If the signal is registered in fluorescence (Alipieva et al., 2003) the signal is mainly from atoms out of the laser beam volume, which interact with the Rayleigh scattered light. In this case the narrow component is Lorentzian and its width is defined by the relaxation time due to atomic collisions with the cell walls.

3. Conclusion

The investigation of the influence of different factors on the shape of the CPT resonances excited in Hanle effect configuration in uncoated, room temperature vacuum cell and registered in fluorescence has shown that the resonance has a complex shape. The performed numerical calculations, which take into account the Gaussian distribution of the laser beam intensity, the experimental geometry of the excitation, the velocity distribution of the atoms, the high rank polarization moment, the stray magnetic fields influence, and the Rayleigh scattering, describe very well the experimental shapes. The results show that the developed theoretical modelling can be applied for analysis of the influence of the different factors and analysis of the cell quality. The Rayleigh scattering can be used for analysis of the vacuum cleanness of the cell and the quality of the cell walls.

On the other hand these narrow resonances can be applied for building magneto-optical sensors. From the point of view of applications in magnetometry, where narrow signals and high signal-to-noise ratios are important, the narrow Rayleigh structure of the CPT resonance measured in fluorescence offer good possibilities: is not power broadened, its width do not depend on the position of the detector and its amplitude increases with the power. The complex structure of the resonance expands the range of the measured magnetic fields.

4. Acknowledgements

The authors are pleased to acknowledge the financial support of part of the investigations by the Bulgarian NCSR (Grant No. DO02-108/22.05.2009).

5. References

Alexandrov, E. B.; Chaika, M. P. & Hvostenko, G. I. (1991). *Interference of atomic states*, Springer-Verlag, ISBN-10: 354053752X, ISBN-13: 978-3540537526

Alipieva, E.; Gateva, S.; Taskova, E. & Cartaleva, S. (2003). Narrow structure in the coherent population trapping resonance in Rb, *Optics Letters*, Vol.28, No.19, pp. 1817-1819, ISSN 0146-9592

Alzetta, G.; Gozzini, A.; Moi, L. & Orriols, G. (1976). An experimental method for the observation of r.f. transitions and laser beat resonances in oriented Na vapour, *Il Nuovo Cimento B Series 11*, Vol.36, No.1, pp. 5-20, ISSN 0369-3546

Arimondo, E. (1996). Coherent population tapping in laser spectroscopy, *Progress in Optics*, Vol.35, pp. 257-354, ISSN 0079-6638

Auzinsh, M.; Budker, D. & Rochester, S.M. (2009a). Light-induced polarization effects in atoms with partially resolved hyperfine structure and applications to absorption, fluorescence, and nonlinear magneto-optical rotation, *Physical Review A - Atomic, Molecular, and Optical Physics*, Vol. 80, No. 5, art. no. 053406, pp. 1-22, ISSN 1050-2947

Auzinsh, M.; Ferber, R.; Gahbauer, F.; Jarmola, A. & Kalvans, L. (2009b). Nonlinear magneto-optical resonances at D1 excitation of Rb 85 and Rb87 for partially resolved hyperfine F levels, *Physical Review A - Atomic, Molecular, and Optical Physics*, Vol. 79 No. 5, art. no. 053404, pp. 1-9, ISSN 1050-2947.

Bison, G; Castanga, N.; Hofer, A.; Knowles, P.; Schenker, J.L.; P., Schenker, J.-L.; Kasprzak, M.; Saudan, H. & Weis, A. (2009). A room temperature 19-channel magnetic field mapping device for cardiac signals. *Applied Physics Letters*, Vol.95, No.17, art. no. 173701, pp. 1-3, ISSN 0003-6951

Bouchiat, M.A. & Brossel, J. (1966). Relaxation of optically pumped rb atoms on paraffin-coated walls. *Physical Review*, Vol.147, No., pp. 41-54, ISSN 0031-899X

Boyd, R. W. (1992). *Nonlinear Optics,* Academic Press, ISBN 0123694701

Budker, D. & Romalis, M. (2007). Optical magnetometry, *Nature Physics,* Vol.3, No.4, pp. 227-234, ISSN 17452473

Carminati, F.-R.; Sanchez-Palencia, L.; Schiavoni, M.; Renzoni, F. & Grynberg, G. (2003). Rayleigh Scattering and Atomic Dynamics in Dissipative Optical Lattices, *Physical Review Letters,* Vol.90, art.no. 043901, ISSN 0031-9007

Corney, A. (1977). *Atomic and Laser Spectroscopy*, Clarendon, Oxford, ISBN 9780198511380

Cox, K.; Yudin, V.I.; Taichnachev, A.V.; Novikova, I. & Mikhailov, E.E. (2011). Measurements of the magnetic field vector using multiple electromagnetically induced transparency resonances in Rb vapor, *Physical Review A - Atomic, Molecular, and Optical Physics*, Vol.83, No.1, art. no. 015801, pp. 1-4, ISSN 1050-2947.

Dancheva, Y.; Alzetta, G.; Cartaleva, S.; Taslakov, M. & Andreeva, Ch. (2000). Coherent effects on the Zeeman sublevels of hyperfine states in optical pumping of Rb by monomode diode laser, *Optics Communications,* Vol.178, No.1, pp. 103-110, ISSN 0030-4018

Dang, H.B.; Maloof, A.C. & Romalis, M.V. (2010). Ultrahigh sensitivity magnetic field and magnetization measurements with an atomic magnetometer, *Applied Physics Letters*, Vol.97, No.15, art. no. 151110, ISSN 0003-6951

Datsyuk, V. M.; Sokolov, I. M.; Kupriyanov, D. V. & Havey, M. D. (2006). Diffuse light scattering dynamics under conditions of electromagnetically induced transparency *Physical Review A - Atomic, Molecular, and Optical Physics,* Vol.74, art.no. 043812, ISSN 0031-9007

Decomps B., Dumont M. & Ducloy M. (1976). *Laser Spectroscopy of Atoms and Molecules*, Springer-Verlag, Berlin, ISBN 3-540-07324-8

D'yakonov, M. I. & Perel, V. I. (1966). On the theory of the gas laser in a magnetic field, *Optics and Spectroscopy*, Vol.20, No.3, pp. 472-480, ISSN 0030-400X

Ducloy, M. & Dumont, M. (1970). Etude du transfert d'excitation par emission spontanee, *Le journal de Physique*, Vol.31, pp. 419-427, ISSN 0302-0738

Edelstein, A. (2007). Advances in magnetometry. *Journal of Physics Condensed Matter*, Vol.19, No.16, art. no. 165217, ISSN 0953-8984.

Firstenberg, O.; Shuker, M.; Ben-Kish, A.; Fredkin, D.R.; Davidson, N. & Ron, A. (2007). Theory of Dicke narrowing in coherent population trapping. *Physical Review A - Atomic, Molecular, and Optical Physics*, Vol. 76, No. 1, art. no. 013818, pp.1-6, ISSN 1050-2947.

Figueroa, E.; Vewinger, F.; Appel, J. & Lvovsky, A.I. (2006) . Decoherence of electromagnetically induced transparency in atomic vapor. *Optics Letters*, Vol.31, No.17, pp. 2625-2627, ISSN 0146-9592

Gao, J.-Y.; Xiao, M. & Zhu, Y. (eds.) (2009). *Atomic coherence and Its Potential Application*, Bentham Science Publishers Ltd., ISBN: 978-1-60805-085-7

Gateva, S.; Alipieva, E. & Taskova, E. (2005). Power dependence of the coherent-population-trapping resonances registered in fluorescence and transmission: Resonance-width narrowing effects. *Physical Review A - Atomic, Molecular, and Optical Physics*, Vol. 72, No.1, art.no. 025805, pp.1-4, ISSN 1050-2947

Gateva, S.; Petrov, L.; Alipieva, E.; Todorov, G.; Domelunksen, V. & Polischuk, V. (2007). Shape of the coherent population-trapping resonances and high-rank polarization moments. *Physical Review A - Atomic, Molecular, and Optical Physics*, Vol. 76, No. 2, art. no. 025401, pp. 1-4, ISSN 1050-2947

Gateva, S.; Alipieva, E.; Petrov, L.; Taskova, E. & Todorov, G. (2008a). Single frequency coherent-population-trapping resonances for magnetic field measurement. *J. Optoelectronics and Advanced Materials,* Vol. 10, No.1, pp. 98-103, ISSN 1454-4164

Gateva, S.; Alipieva, E.; Domelunksen, V.; Polischuk, V.; Taskova, E.; Slavov, D.; Todorov, G. (2008b). Shape of the coherent-population-trapping resonances registered in fluorescence at different experimental geometries. *Proceedings of SPIE - The International Society for Optical Engineering*, Vol. 7027, art. no. 70270I, pp. 1-12, ISBN 9780819472410.

Gateva, S.; Gurdev, L.; Alipieva, E.; Taskova, E. & Todorov, G. (2011). Narrow structure in the coherent population trapping resonances in rubidium and Rayleigh scattering. *Journal of Physics B: Atomic, Molecular and Optical Physics,* Vol. 44, No. 3, art. no. 035401, pp. 1-6 , ISSN 0953-4075

Godone, A.; Levi, F.; Micalizio, S. & Vanier, J. (2002). Dark-line in optically-thick vapors: Inversion phenomena and line width narrowing, *The European Physical Journal D*, Vol.18, No.1, pp. 5-13, ISSN 1434-6060

Gozzini, S.; Marmugi, L.; Lucchesini, A.; Gateva, S.; Cartaleva, S. & Nasyrov, K. (2011). Narrow structure in the coherent population trapping resonance in sodium, *Physical Review A - Atomic, Molecular, and Optical Physics*, Vol. 84, No. 1, art. no. 013812, pp. 1-9, ISSN 1050-2947

Griffith, W.C.; Knappe, S. & Kitching, J. (2010). Femtotesla atomic magnetometry in a microfabricated vapor cell, *Optics Express*, Vol.18, No.26, pp. 27167-27172, ISSN 1094-4087.

Huss, A.; Lammegger, R.; Windholz, L.; Alipieva, E.; Gateva, S.; Petrov, L.; Taskova, E. & Todorov, G. (2006). Polarization-dependent sensitivity of level-crossing, coherent-population-trapping resonances to stray magnetic fields. *Journal of the Optical Society of America B: Optical Physics*, Vol.23, no.9, pp. 1729-1736, ISSN 0740-3224

Javan, A.; Kocharovskaya, O.; Lee, H. & Scully, M.O. (2002). Narrowing of electromagnetically induced transparency resonance in a Doppler-broadened medium. *Physical Review A - Atomic, Molecular, and Optical Physics*, Vol.66, No. 1, pp. 138051-138054, ISSN 1050-2947

Johnson, C.; Schwindt, P.D.D. & Weisend, M. (2010). Magnetoencephalography with a two-color pump-probe, fiber-coupled atomic magnetometer. *Applied Physics Letters*, Vol.97, No.24, art. no. 243703, ISSN 0003-6951

Kimble, H.J. (2008). The quantum internet. *Nature*, Vol.453, pp. 1023-1030, ISSN 0028-0836

Kitching, J.; Knappe, S. & Donley, E.A. (2011). Atomic sensors - A review. *IEEE Sensors Journal*, Vol. 11, No.9, art. no. 5778937, pp. 1749-1758. ISSN 1530-437X.

Knappe, S.; Wynands, R.; Kitching, J.; Robinson, H. G. & Hollberg, L. (2001). Characterization of coherent population-trapping resonances as atomic frequency

references, *Journal of the Optical Society of America B: Optical Physics*, Vol.18, No.11, pp. 1545-1553, ISSN 0740-3224

Knappe, S.; Shah, V.; Schwindt, P.D.D.; Hollberg, L.; Kitching, J.; Liew, L. & Moreland, J. (2004). Microfabricated atomic clock, *Applied Physics Letters,* Vol. 85, No. 9, pp. 1460-1462, ISSN 0003-6951

Knappe, S.; Sander, T.M.; Kosch, O.; Wiekhorst, F.; Kitching, J. & Trahms, L. (2010). Cross-validation of microfabricated atomic magnetometers with superconducting quantum interference devices for biomagnetic applications, *Applied Physics Letters,* Vol. 97, art. no. 133703, pp. 1-3, ISSN 0003-6951

Kominis, I. K.; Kornack, T. W.; Allred, J. C. & Romalis, M. V. (2003). A subfemtotesla multichannel atomic magnetometer. *Nature,* Vol. 422, No.6932, pp. 596-599, ISSN 0028-0836

Landau, L.D. & Lifshitz, E.M. (1965). *Quantum Mechanics: Non-Relativistic Theory*, Pergamon Press, ISBN 978-0-080-20940-1

Levi, F.; Godone, A.; Vanier, J.; Micalizio, S. & Modugno, G. (2000). Line-shape of dark line and maser emission profile in CPT. *The European Physical Journal D*, Vol.12, No.1, pp. 53-59, ISSN 1434-6060

Lukin, M.D. (2003). Colloquium: Trapping and manipulating photon states in atomic ensembles. *Reviews of Modern Physics*, Vol.75, pp. 457-472, ISSN 0034-6861

Matsko, A. B.; Novikova, I.; Scully, M. O. & Welch, G. R. (2001). Radiation trapping in coherent media. *Physical Review Letters,* Vol.87, No.13, art. no. 133601, ISSN 1079-7114

Measures, R. M. (1984). *Laser Remote Sensing*: *Fundamentals and Applications,* Wiley ISBN 0471081930 (ISBN13: 9780471081937), New York

Mikhailov, E.; Novikova, I,; Havey, M.D. & Narducci, F.A. (2009). Magnetic field imaging with atomic Rb vapour. *Optics Letters*, Vol.34, No.22, pp. 3529-3531, ISSN 0146-9592

Okunevich, A. I., (2001). On the possibility of registration of hexadecapole transversal components of the atoms in fluorescence. *Optics and Spectroscopy*, Vol.91, No.2, pp. 193-200, ISSN 0030-400X

Petrov, L.; Slavov, D.; Arsov, V.; Domelunksen, V.; Polischuk, V. & Todorov, G. (2007) High rank polarization moments in a Doppler broadened 87Rb transition, *Proceedings of SPIE - The International Society for Optical Engineering*, Vol. 6604, pp. 66040H1-66040H5, ISBN 9780819467423

Pfleghaar, E.; Wurster, J.; Kanorsky, S.I. & Weis, A. (1993). Time of flight effects in nonlinear magneto-optical spectroscopy, *Optics Communications*, Vol. 99, No. 5-6, pp. 303-308. ISSN 0030-4018.

Polischuk, V.; Domelunksen, V.; Alipieva, E. & Todorov, G. (2011). MatLab based modelling of nonlinear interaction of Rb87 atoms with polarized radiation. *unpublished*

Romalis, M.V. & Dang, H.B. (2011). Atomic magnetometers for materials characterization. *Materials Today,* Vol.14, no.6, pp. 258-262, ISSN 1369-7021

Savukov, I. (2010). Ultra-Sensitive Optical Atomic Magnetometers and Their Applications, In: *Advances in Optical and Photonic Devices,* Ki Young Kim, (Ed.), 329-352, InTech, ISBN 978-953-7619-76-3, Croatia

Steck, D.A. (2009) *Rubidium 87 D Line Data* (available online http://steck.us/alkalidata)

Taichenachev, A.V.; Tumaikin, A. M.; Yudin, V. I.; Stähler, M.; Wynands, R.; Kitching, J. & Hollberg L. (2004). Nonlinear-resonance line shapes: Dependence on the transverse

intensity distribution of a light beam. *Physical Review A - Atomic, Molecular, and Optical Physics,* Vol.69, art. no. 024501, ISSN 1050-294711

Thomas, J. E. & Quivers, W. W. (1980). Transit-time effects in optically pumped coupled three-level systems, *Physical Review A - Atomic, Molecular, and Optical Physics* 22(5), 2115-2121, ISSN 1050-294711

Xia, H.; Baranga, A.B.-A.; Hoffman, D. & Romalis, M.V. (2006). Magnetoencephalography with an atomic magnetometer. *Applied Physics Letters*, Vol.89, art. no. 211104, ISSN 0003-6951

Xiao, Y.; Novikova, I.; Phillips, D. F. & Walsworth, R. L. (2006) Diffusion-Induced Ramsey Narrowing. *Physical Review Letters,* Vol.96, art. no. 043601, ISSN 1079-7114

Xiao, Y.; Novikova, I.; Phillips, D. F. & Walsworth, R. L. (2008). Repeated interaction model for diffusion-induced Ramsey narrowing, *Optics Express,* Vol.16, pp. 14128-14141, ISSN 1094-4087

Xu, S.; Crawford, C.W.; Rochester, S.; Yashchuk, V.; Budker, D. & Pines, A. (2008). Submillimeter-resolution magnetic resonance imaging at the Earth's magnetic field with an atomic magnetometer. *Physical Review A - Atomic, Molecular, and Optical Physics,* Vol. 78 No.1, art. no. 013404, pp. 1-4, ISSN 1050-294711.

Ye, C.Y. & Zibrov, A. S. (2002). Width of the electromagnetically induced transparency resonance in atomic vapor. *Physical Review A - Atomic, Molecular, and Optical Physics,* Vol. 65, No. 2, art.no. 023806, pp. 1-5, ISSN 1050-2947

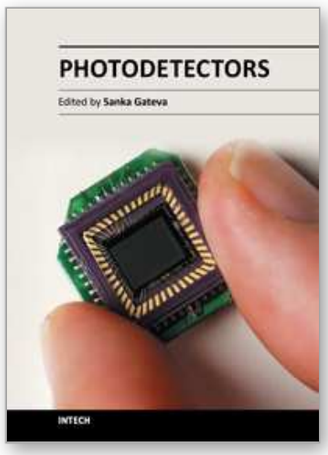

Photodetectors

Edited by Dr. Sanka Gateva

ISBN 978-953-51-0358-5
Hard cover, 460 pages
Publisher InTech
Published online 23, March, 2012
Published in print edition March, 2012

In this book some recent advances in development of photodetectors and photodetection systems for specific applications are included. In the first section of the book nine different types of photodetectors and their characteristics are presented. Next, some theoretical aspects and simulations are discussed. The last eight chapters are devoted to the development of photodetection systems for imaging, particle size analysis, transfers of time, measurement of vibrations, magnetic field, polarization of light, and particle energy. The book is addressed to students, engineers, and researchers working in the field of photonics and advanced technologies.

How to reference

In order to correctly reference this scholarly work, feel free to copy and paste the following:

Sanka Gateva and Georgi Todorov (2012). Shape of the Coherent Population Trapping Resonances Registered in Fluorescence, Photodetectors, Dr. Sanka Gateva (Ed.), ISBN: 978-953-51-0358-5, InTech, Available from: http://www.intechopen.com/books/photodetectors/shape-of-the-coherent-population-trapping-resonances-registered-in-fluorescence

INTECH
open science | open minds

InTech Europe
University Campus STeP Ri
Slavka Krautzeka 83/A
51000 Rijeka, Croatia
Phone: +385 (51) 770 447
Fax: +385 (51) 686 166
www.intechopen.com

InTech China
Unit 405, Office Block, Hotel Equatorial Shanghai
No.65, Yan An Road (West), Shanghai, 200040, China
中国上海市延安西路65号上海国际贵都大饭店办公楼405单元
Phone: +86-21-62489820
Fax: +86-21-62489821

IntechOpen